# Theoretical Analysis of Binary Masks in Snapshot Compressive Imaging Systems

Mengyu Zhao

Abstract—Snapshot compressive imaging (SCI) systems have gained significant attention in recent years. While previous theoretical studies have primarily focused on the performance analysis of Gaussian masks, practical SCI systems often employ binary-valued masks. Furthermore, recent research has demonstrated that optimized binary masks can significantly enhance system performance. In this paper, we present a comprehensive theoretical characterization of binary masks and their impact on SCI system performance. Initially, we investigate the scenario where the masks are binary and independently identically distributed (iid), revealing a noteworthy finding that aligns with prior numerical results. Specifically, we show that the optimal probability of non-zero elements in the masks is smaller than 0.5. This result provides valuable insights into the design and optimization of binary masks for SCI systems, facilitating further advancements in the field. Additionally, we extend our analysis to characterize the performance of SCI systems where the mask entries are not independent but are generated based on a stationary first-order Markov process. Overall, our theoretical framework offers a comprehensive understanding of the performance implications associated with binary masks in SCI systems.

## I. INTRODUCTION

Snapshot compressive imaging (SCI) refers to imaging systems that are designed to map a high-dimensional (HD) 3D data cube into a 2D image through hardware. (Refer to Fig. 1 for a schematic model of SCI systems encoding function.) The desired HD 3D data cube is then recovered from the 2D projection using proper algorithms. The motivation behind developing SCI solutions is to make the data acquisition phase more efficient. For instance, a key application of SCI is in hyperspectral imaging (HSI). HSI is an emerging technology with a wide range of applications, from medicine to astronomy, see e.g. [1]–[5]. The key challenge with classic HSI solutions is that they rely on scanning the image either in space or along the wavelengths. This makes the HSI process slow and costly. To address this challenge, a snapshot compressive hyperspectral imaging solution has been proposed that can dramatically speed up the process by capturing all the information in a single snapshot [6].

In recent years, numerous hardware solutions for SCI have been proposed for various applications (for an overview, refer to [7]). As shown in Fig. 1, the encoding operation of SCI systems can be modeled as highly under-determined linear inverse problems with specialized sensing matrices. Various methods have been proposed in the literature for solving such inverse problems., e.g. see [8]–[12]. While SCI systems are under-

MZ is with the Electrical and computer Engineering Department of Rutgers University. E-mail: mz524@soe.rutgers.edu

SJ is with the Electrical and computer Engineering Department of Rutgers University. E-mail: shirin.jalali@rutgers.edu

Shirin Jalali

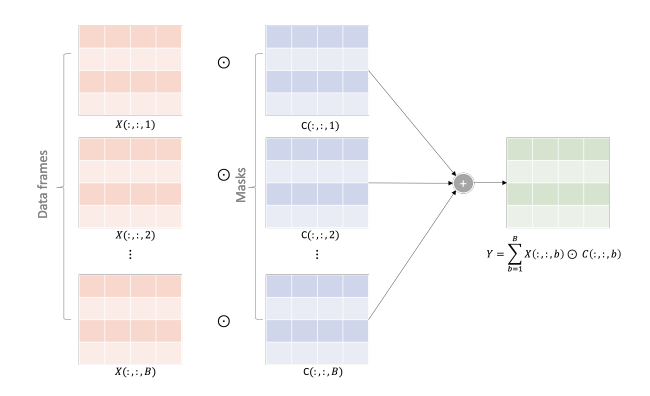


Fig. 1. SCI encoding function: For  $b=1,\ldots,B$ , frame b and mask b are represented by X(:,:,b) and C(:,:,b), respectively. The single 2D measurement frame is generated as  $\sum_{b=1}^B X(:,:,b) \odot C(:,:,b)$ .

determined linear inverse problems, the specialized structure of their sensing matrices on one hand, and the complex structure of the input data on the other hand, prevents results from compressed sensing to be directly applicable to such systems. Therefore, for theoretical analysis of such systems new tools and techniques are required. Such a theoretical analysis is performed in [13], for the case where the corresponding linear mapping can be modeled as a highly sparse matrix with its non-zero entries distributed as i.i.d. Gaussian. The analysis of [13] theoretically shows that recovery of the signal from SCI measurements is indeed feasible. However, practical SCI systems often employ binary-valued (or finite-valued) masks. Also, in many practical cases, the masks corresponding to different frames are not independent and are instead (sometimes randomly [14]) shifted versions of each other. These raise the following questions.

**Question 1.** For binary-valued masks, can we theoretically characterize the performance of the SCI system in terms of the statistical properties of the masks, e.g., the probability of non-zero entries, or the correlation between adjacent (inframe or out-of-frame) values? If the answer is positive, can we use these theoretical results to theoretically optimize the performance of the system?

**Question 2.** How does the dependency between the masks used for different frames affect the achievable SCI performance? For a specified type of dependence between the masks, e.g., randomly shifted masks, can we optimize the initial mask, such that the achievable performance is optimized?

The goal of this paper is to address these questions. To

achieve this goal we adopt the compression-based optimization, compressible signal pursuit (CSP), initially proposed in [15] and later utilized in [13] for the theoretical analysis of SCI systems. Within this framework, we make the following main contributions:

- 1) Theoretical characterization of CSP optimization performance for SCI recovery under i.i.d. binary masks. Our analysis reveals that the probability of non-zero entries minimizing the achieved distortion is less than 0.5.
- 2) Theoretical characterization of CSP optimization performance for scenarios where non-zero entries in each frame exhibit dependence, following a binary first-order Markov process. In this case, we assume that the nonzero entries of different masks are independent.
- Investigation of the impact of dependency across frames by studying cases where entries across frames are dependent, aiming to model the effect of mask dependence.

#### A. Related work

Recent research has focused on optimizing masks to enhance the performance of SCI systems. Trained sensing binary masks have been explored, demonstrating notable improvements over random mask designs [16]. These optimized binary masks have a nonzero element probability of around 40 percent and exhibit smooth variations. Deep unfolding networks have also been employed to simultaneously reconstruct hyperspectral images and optimize mask designs, resulting in preserved image structure and optimal sampling [17]. Furthermore, a comparison between random masks and optimized masks, validated with hardware prototypes, supports the benefits of optimization [18]. Other approaches include incorporating apertures for mask multiplexing [19] and using end-to-end networks to jointly optimize masks and networks, leading to improved loss function and peak signal-to-noise ratio (PSNR) performance [20]. Collectively, these studies highlight the impact of mask optimization in enhancing SCI system performance.

## B. Notations

Vectors are denoted by bold letters, such as  $\mathbf{x}$  and  $\mathbf{y}$ . For a matrix  $\mathbf{X} \in \mathbb{R}^{n_1 \times n_2}$ ,  $\operatorname{Vec}(\mathbf{X})$  denotes the vector in  $\mathbb{R}^n$ ,  $n = n_1 \times n_2$ , formed by concatenating the columns of  $\mathbf{X}$ .  $\odot$  denotes the Hadamard matrix product operator defined as follows. For  $\mathbf{A}, \mathbf{B} \in \mathbb{R}^{n_1 \times n_2}$ ,  $\mathbf{Y} = \mathbf{A} \odot \mathbf{B}$  is defined such that  $Y_{ij} = A_{ij}B_{ij}$ , for all i, j. Sets are denoted by calligraphic letters, such as  $\mathcal{A}, \mathcal{B}$ . For a finite set  $\mathcal{A}, |\mathcal{A}|$  denotes the size of  $\mathcal{A}$ 

## C. Outline

The mathematical models of SCI systems encoding and decoding operations are described in Section II. Section III reviews the idea of compression-based methods for solving SCI inverse problems. The main theoretical results of the paper are presented in Section IV and the proofs are presented in Section V. Section VI concludes the paper.

## II. PROBLEM STATEMENT

The goal of an SCI system is to recover a 3D data cube from its 2D projection, while knowing the mapping. More precisely, let  $\mathbf{X} \in \mathbb{R}^{n_1 \times n_2 \times B}$  denote the desired 3D data cube. An SCI system maps  $\mathbf{x}$  to a single measurement frame  $\mathbf{Y} \in \mathbb{R}^{n_1 \times n_2}$ . In many SCI systems, such as HS SCI [6] and video SCI [14], the mapping from  $\mathbf{X}$  to  $\mathbf{Y}$  can be modeled as a linear system such that [14], [21],  $\mathbf{Y} = \sum_{b=1}^{B} \mathbf{C}_b \odot \mathbf{X}_b + \mathbf{Z}$ , where  $\mathbf{C} \in \mathbb{R}^{n_1 \times n_2 \times B}$  and  $\mathbf{Z} \in \mathbb{R}^{n_1 \times n_2}$  denote the sensing kernel (mask) and the additive noise, respectively. Here,  $\mathbf{C}_b = \mathbf{C}(:,:,b)$  and  $\mathbf{X}_b = \mathbf{X}(:,:,b) \in \mathbb{R}^{n_1 \times n_2}$  represent the b-th sensing kernel (mask) and the corresponding signal frame, respectively; Here,  $\odot$  denotes the Hadamard or element-wise product.

To simplify the mathematical representation of the system, we vectorize each frame as  $\mathbf{x}_b = \mathrm{Vec}(\mathbf{X}_b) \in \mathbb{R}^n$  with  $n = n_1 n_2$ . Then, we vectorize the data cube  $\mathbf{X}$  by concatenating the B vectorized frames into a column vector  $\mathbf{x} \in \mathbb{R}^{nB}$  as

$$\mathbf{x} = \begin{bmatrix} \mathbf{x}_1 \\ \vdots \\ \mathbf{x}_B \end{bmatrix}. \tag{1}$$

Similarly, we define  $\mathbf{y} = \text{Vec}(\mathbf{Y}) \in \mathbb{R}^n$  and  $\mathbf{z} = \text{Vec}(\mathbf{Z}) \in \mathbb{R}^n$ . Using these definitions, the measurement process defined in Fig. 1 can also be expressed as

$$y = Hx + z. (2)$$

The sensing matrix  $\mathbf{H} \in \mathbb{R}^{n \times nB}$ , is a highly sparse matrix that is formed by the concatenation of B diagonal matrices as

$$\mathbf{H} = [\mathbf{D}_1, ..., \mathbf{D}_B],\tag{3}$$

where, for b = 1, ... B,  $\mathbf{D}_b = \operatorname{diag}(\operatorname{Vec}(\mathbf{C}_b)) \in \mathbb{R}^{n \times n}$ . The goal of a SCI recovery algorithm is to recover the data cube  $\mathbf{x}$  from undersampled measurements  $\mathbf{y}$ , while having access to the sensing matrix (or mask)  $\mathbf{H}$ .

## III. COMPRESSION-BASED SCI RECOVERY

One of the key challenges in theoretical analysis of SCI systems is developing a mathematical model for the structure of 3D data cubes, such as videos or HS images. On approach to address this issue is to use the idea of compression-based recovery, which was initially proposed in [15] in the context of compressed sensing. In that case, it can be shown that at least in cases where the minimum achievable sample rate is known, compression-based methods are able to achieve it [22]. Inspired by this idea, in [13], the first theoretical analysis of SCI systems was performed using data compression codes for capturing the source structure.

Compression codes designed for a class of signals are designed to take advantage of the structure of the signals in that class to represent it as efficiently as possible. The key idea of using compression codes for solving inverse problems is to use the compression code as a black-box that implicitly takes advantage of signal structure. In the following we briefly review some key definitions related to compression codes defined for a given class of HD data cubes.

Consider a compact set  $\mathcal{Q} \subset \mathbb{R}^{nB}$ . Each signal  $\mathbf{x} \in \mathcal{Q}$ , consists of B vectors (frames)  $\{\mathbf{x}_1 \dots \mathbf{x}_B\}$  in  $\mathbb{R}^n$ . A lossy compression code of rate r for  $\mathcal{Q}$  is characterized by its encoding mapping f, where  $f: \mathcal{Q} \to \{1, 2, \dots, 2^{Br}\}$ , and  $g: \{1, 2 \dots 2^{Br}\} \to \mathbb{R}^{nB}$ . For  $\mathbf{x} \in \mathcal{Q}$ ,  $\tilde{\mathbf{x}} = g(f(\mathbf{x}))$  denotes the reconstruction corresponding to  $\mathbf{x}$ . The *distortion* between  $\mathbf{x}$  and its reconstruction  $\hat{\mathbf{x}}$  is defined as

$$d(\mathbf{x}, \hat{\mathbf{x}}) \triangleq \|\mathbf{x} - \hat{\mathbf{x}}\|_2^2. \tag{4}$$

The compression code (f,g) is characterized by its rate r and distortion  $\delta$  defined as

$$\delta = \sup_{\mathbf{x} \in \mathcal{O}} d(\mathbf{x}, g(f(\mathbf{x}))).$$

Moreover, the defined encoder and decoder pair, (f,g), correspond to a codebook  $\mathcal C$  defined as

$$C = \{g(f(\mathbf{x})) : \mathbf{x} \in Q\}. \tag{5}$$

Note that  $|\mathcal{C}| < 2^{Br}$ .

Consider the problems of SCI defined in Section III. To recover  $\mathbf x$  from underdetermined measurements  $\mathbf y$ , we need to take advantage of the structure of  $\mathbf x$ . However, as explained earlier, the desired mathematical model of the structure needs to capture both intra- on inter-frame dependencies, which makes designing such models inherently very complex. One approach to address this issue and provide a theoretical analysis is SCI systems is to adopt the idea of compression-based recovery. The key advantage of this approach is that instead of explicitly expressing the structure, it will be captured through a compression code, and the performance is determined by the key parameters of the compression code, i.e., its rate r and distortion  $\delta$ .

Given a class of signal denoted by a  $\mathcal{Q} \subset \mathbb{R}^{nB}$ , and a rate-r distortion- $\delta$  compression code (f,g), the compressible signal pursuit (CSP) optimization recovers  $\mathbf{x} \in \mathcal{Q}$  from measurements  $\mathbf{y} \in \mathbb{R}^n$  defined in (2), as follows

$$\hat{\mathbf{x}} = \arg\min_{\mathbf{c} \in \mathcal{C}} \|\mathbf{y} - \sum_{i=1}^{B} \mathbf{D}_{i} \mathbf{c}_{i}\|_{2}^{2}.$$
 (6)

The performance of (6) is theoretically characterized in [13] for the case where the diagonal entries of  $\mathbf{D}_1, \dots, \mathbf{D}_B$  are i.i.d. Gaussian. In this paper, inspired by used in practical SCI systems, we focus on the case of binary-valued masks, and under various distributions characterize the performance of (6).

## IV. CHARACTERIZATION OF EFFECT OF MASKS

In this section, we present our main theoretical results on the performance of SCI systems under different settings of binary masks. Our goal is to address the questions we raised before on how the statistical properties and dependencies of binary masks impact the performance of SCI systems, and whether it is possible to optimize the masks to achieve better performance. We discuss our findings in three distinct settings, each corresponding to different mask characteristics and their effects on the system's performance.

## A. i.i.d. Bernoulli masks

As the first scenario, we focus on the masks entries are i.i.d. and binary-valued. There are two key questions we want to address in this setting: Is recovery still feasible? If so, what is the optimal value of p,  $p = P(D_{ij} = 1)$ , that minimizes the achieved distortion between the signal and its SCI reconstruction?

**Theorem 1.** Consider  $Q \subset \mathbb{R}^{nB}$ , where for all  $\mathbf{x} \in Q$ ,  $\|\mathbf{x}\|_{\infty} \leq \frac{\rho}{2}$ . Let C denote the codebook corresponding to a rate-r distortion- $\delta$  lossy compression code for signals in Q. Assume that  $\mathbf{D}_1 \dots \mathbf{D}_B$  are such that  $\mathbf{D}_i = \operatorname{diag}(D_{i1} \dots D_{in})$ ,  $i = 1, \dots, B$ , where the diagonal entries of the matrices drawn independently i.i.d.  $\operatorname{Bern}(p)$ . For  $\mathbf{x} \in Q$  and  $\mathbf{y} = \sum_{i=1}^{B} \mathbf{D}_i \mathbf{x}_i$  let  $\hat{\mathbf{x}}$  denote the solution of (6). Choose free parameter  $\epsilon > 0$ . Then,

$$\frac{1}{nB} \|\mathbf{x} - \hat{\mathbf{x}}\|_{2}^{2} \le \left(1 + \frac{Bp}{1-p}\right) \left(\frac{\delta}{nB}\right) + \frac{\rho^{2}B\epsilon}{(p-p^{2})},\tag{7}$$

with a probability larger than  $1-2^{Br+1}\exp(-n\epsilon^2/2)$ . Moreover, for fixed parameters  $(n, B, \epsilon, \rho)$ , the bound in (7) is minimized at some  $p^*$ , where  $p^* < \frac{1}{2}$ .

Note that as  $p \to 0$  or  $p \to 1$ , the bound in (7) grows without bound. This is consistent with the fact that we cannot expect recovery from all-zero or all-one masks. On the other hand, for p = 0.5, Theorem 1 guarantees that

$$\frac{1}{nB} \|\mathbf{x} - \hat{\mathbf{x}}\|_2^2 \le (1+B)(\frac{\delta}{nB}) + 4\rho^2 \epsilon,$$

with probability larger than  $1-2^{Br+1}\exp(-\frac{n\epsilon^2}{2B^2})$ . Moreover, it states that the optimal  $p^*$  is smaller than 0.5, which means that the optimal bound is tighter than this result. This is consistent with the results from the literature, e.g. [16], that show through various types of algorithmic optimizations that in the learned optimized binary masks  $P(D_{ij}=1)$  is strictly smaller than 0.5.

One distinctive property of the studied masks compared to i.i.d. Gaussian masks studied in the prior art is that  $D_{i,j} \geq 0$ , w.p. 1. To further highlight this difference and show its potential impact on optimizing the masks, in the following corollary of Theorem 1, we consider the case where instead of binary-valued, the masks take values in  $\{-1, +1\}$ . In that case, we see that unlike the case of binary masks, the optimal bound on the distortion is achieved for the case where p=0.5 and  $\mathrm{E}[D_{i,j}]=0$ .

**Corollary 1.** Consider the same setup as in Theorem 1, where instead of binary masks,  $D_{ij} \in \{-1, +1\}$  and  $\{\{D_{ij}\}_{j=1}^n\}_{i=1}^B$  are i.i.d. such that  $P(D_{ij} = 1) = 1 - P(D_{ij} = -1) = p$ . Then

$$\frac{1}{nB} \|\mathbf{x} - \hat{\mathbf{x}}\|_{2}^{2} \le \frac{4(p-p^{2})(1-B) + B}{4(p-p^{2})} (\frac{\delta}{nB}) + \frac{\rho^{2}\epsilon}{4(p-p^{2})},$$

with a probability larger than  $1-2^{Br+1}\exp(-\frac{n\epsilon^2}{2B^2})$ . Moreover, the upper bound is minimized at  $p^*=\frac{1}{2}$ , which leads to  $\frac{1}{nB}\|\mathbf{x}-\hat{\mathbf{x}}\|_2^2 \leq \frac{1}{nB}\delta + \rho^2\epsilon$ .

## B. Binary Markov masks: in-frame dependence

As the first model of masks with dependent components, we consider a setting where masks corresponding to different frames are independent, but the entries of each mask are dependent and follow a first-order Markov process. More precisely, we assume that  $\mathbf{D}_1, \ldots, \mathbf{D}_B$  are independent. For  $i = 1, \ldots, B$ , the diagonal entries of  $\mathbf{D}_i$  are generated according to a stationary Markov process such that, for  $j = 2, \ldots, n$ ,

$$p_{D_{ij}|D_{i,1:(j-1)}}(\cdot|\cdot) = p_{D_{ij}|D_{i,j-1}}(\cdot|\cdot).$$

Moreover, for any i = 1, ..., B, and j = 2, ..., n, we define the transition kernel of the (asymmetric) Markov chain as follows

$$P(D_{ij} = 1 | D_{i(j-1)} = 0) = q_0,$$
  

$$P(D_{ij} = 0 | D_{i(j-1)} = 1) = q_1.$$
(8)

To characterize the performance under the described Markov model for the masks, we use the concentration of measure results developed in [23]. For using that result, we define the contraction coefficient corresponding to the defined Markov process as

$$\theta_{1} = \sup_{\mathbf{d}', \mathbf{d}'' \in \mathcal{S}^{B}} \|p(\cdot|\mathbf{d}') - p(\cdot|\mathbf{d}'')\|_{\text{TV}}$$

$$= \|p_{i}(\cdot|\mathbf{d}' = \mathbf{0}_{B}) - p_{i}(\cdot|\mathbf{d}'' = \mathbf{1}_{B})\|_{\text{TV}}$$

$$= \frac{1}{2} [|q_{0}^{B} - (1 - q_{1})^{B}| + {B \choose 1} |(1 - q_{0})q_{0}^{B-1} - q_{1}(1 - q_{1})^{B-1}| + {B \choose 2} |(1 - q_{0})^{2}q_{0}^{B-2} - q_{1}^{2}(1 - q_{1})^{B-2}| + \dots + |(1 - q_{0})^{B} - q_{1}^{B}|]. \tag{9}$$

In (9), for  $\mathbf{d}, \mathbf{d}' \in \mathcal{S}^B$ ,  $p(\mathbf{d}'|\mathbf{d}) = \prod_{i=1}^B p(d_i'|d_i)$  denotes the transition kernel of the defined Markov process. Fig. 2 shows the value of  $\theta_1$  as a function of  $q_1$ , for a couple of different values of  $q_0$  and B.

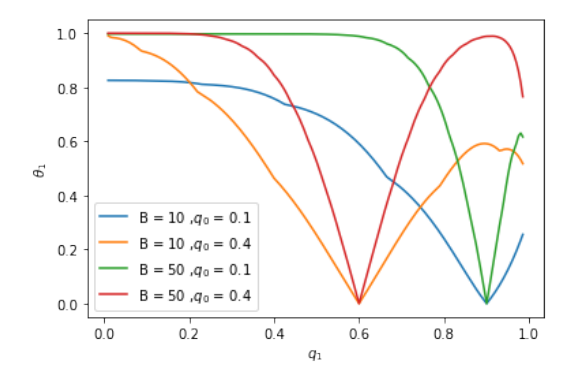


Fig. 2.  $\theta_1$  as a function of  $q_1$ .

**Theorem 2.** Assume that  $\mathbf{D}_1 \dots \mathbf{D}_B$  are such that  $\mathbf{D}_i = \operatorname{diag}(D_{i1} \dots D_{in})$ ,  $i = 1, \dots, B$ , where  $D_{ij} \in \{0, 1\}$ . Assume

that  $(D_{i1}, \ldots, D_{in})$ ,  $i = 1, \ldots, B$ , are independently generated as stationary first order Markov processes with transition probabilities described in (8). For  $\mathbf{x} \in \mathcal{Q}$  and  $\mathbf{y} = \sum_{i=1}^{B} \mathbf{D}_{i} \mathbf{x}_{i}$  let  $\hat{\mathbf{x}}$  denote the solution of (6). Then

$$\frac{1}{nB} \|\mathbf{x} - \hat{\mathbf{x}}\|_{2}^{2} \le (1 + \frac{Bp}{1-p})(\frac{\delta}{nB}) + \frac{\rho^{2}\epsilon}{p(1-p)},\tag{10}$$

with a probability larger than

$$1 - (2^{Br} + 1) \exp(-\frac{n\epsilon^2}{32}(1 - \theta_1)^2),$$

where  $\theta_1$  is defined in (9).

Comparing the bound in (10) and the one in (7) shows that they are indeed equivalent. Therefore, similar to Theorem 1, the bound is minimized for some  $p^* = \frac{q_0^*}{q_0^* + q_1^*} < 0.5$ . On the other hand, to minimize  $\exp(-\frac{n\epsilon^2}{32}(1-\theta_1)^2)$  which controls how many frames can be decoupled from each other, we need to minimize  $\theta_1$  defined in (9). But we can set  $\theta_1 = 0$ , by setting  $q_0^* = p^*$  and  $q_1^* = 1 - p^*$ . It is straightforward to see that setting the parameters  $q_0$  and  $q_1$  as such corresponds to making the Markov process an independent process. This is intuitively not surprising as using this setting the convergence speed of the random variables is maximized.

## C. Binary Markov masks: Out-of-frame dependence

Next we consider the case where the entries of each mask are generated independently, but the mask entries corresponding to element i of each frame are dependent. This is closely related to real masks used in practice where each mask can be a shifted version of the previous mask. Mathematically, we assume that  $D_{1j}, \ldots, D_{Bj}$  are generated according to a stationary first order Markov process such that for any  $j=1,\ldots,n$  and  $i=2,\ldots,B$ ,

$$p_{D_{i,i}|D_{1:(i-1),i}}(\cdot|\cdot) = p_{D_{i,i}|D_{i-1,i}}(\cdot|\cdot),$$

and

$$P(D_{ij} = 1 | D_{i-1,j} = 0) = q_0$$
  

$$P(D_{ij} = 0 | D_{i-1,j} = 1) = q_1.$$
(11)

Assume that  $q_0, q_1 \leq 0.5$  and let

$$\alpha = 1 - q_0 - q_1.$$

Note that since  $q_0, q_1 \leq 0.5$ ,  $\alpha \geq 0$ . Define  $B \times B$  matrix  $\Lambda$  as follows

$$\Lambda = \begin{bmatrix}
1 & \alpha & \cdots & \alpha^{B-1} \\
\alpha & 1 & \cdots & \alpha^{B-2} \\
\vdots & \vdots & \ddots & \vdots \\
\alpha^{B-1} & \alpha^{B-2} & \cdots & 1.
\end{bmatrix} .$$
(12)

Let  $\lambda_{\max}(\Lambda)$  and  $\lambda_{\min}(\Lambda)$  denote the maximum and minimum eigenvalues of matrix  $\Lambda$ , respectively.

**Theorem 3.** Assume that  $\mathbf{D}_1 \dots \mathbf{D}_B$  are such that  $\mathbf{D}_i = \operatorname{diag}(D_{i1} \dots D_{in})$ ,  $i = 1, \dots, B$ , where  $D_{ij} \in \{0, 1\}$ . Assume

that  $(D_{1j}, \ldots, D_{Bj})$ ,  $j = 1, \ldots, n$ , are independently generated as stationary first order Markov processes according to (11). For  $\mathbf{x} \in \mathcal{Q}$  and  $\mathbf{y} = \sum_{i=1}^{B} \mathbf{D}_{i}\mathbf{x}_{i}$  let  $\hat{\mathbf{x}}$  denote the solution of (6). Then, if  $\lambda_{\min}(\Lambda) > 0$ ,

$$\frac{1}{nB} \|\mathbf{x} - \hat{\mathbf{x}}\|_{2}^{2} \leq \frac{\lambda_{\max}(\Lambda)(1-p) + pB}{\lambda_{\min}(\Lambda)(1-p)} (\frac{\delta}{nB}) + \frac{\rho^{2}\epsilon}{\lambda_{\min}(\Lambda)p(1-p)},$$

with a probability larger than  $1 - 2^{Br+1} \exp(-\frac{n\epsilon^2}{2B^2})$ .

Note that in the case where all the entries of the sensing matrix are independent, i.e., the case where  $q_0+q_1=1$  and  $\alpha=0,\ \lambda_{\max}(\Lambda)=\lambda_{\min}(\Lambda)=1$ . Therefore, in that case the upper bound in Theorem 3 simplifies to the result of Theorem 1.

We can use Gershgorin circle theorem [24] to derive upper and lower bounds on  $\lambda_{\max}(\Lambda)$  and  $\lambda_{\min}(\Lambda)$ , respectively, and find the following corollary.

**Corollary 2.** Consider the same setup as in Theorem 3. Then, for  $\alpha < \frac{1}{3}$ ,

$$\begin{split} \frac{1}{nB} \|\mathbf{x} - \hat{\mathbf{x}}\|_2^2 \leq & \frac{(1+\alpha)(1-p) + pB}{(1-3\alpha)(1-p)} (\frac{\delta}{nB}) \\ & + \frac{\rho^2(1-\epsilon)}{(1-3\alpha)p(1-p)}, \end{split}$$

with a probability larger than  $1 - 2^{Br+1} \exp(-\frac{n\epsilon^2}{2B^2})$ .

## V. Proofs

## A. Proof of Theorem 1

Let  $\tilde{\mathbf{x}} = g(f(\mathbf{x}))$ . By assumption, the code operates at distortion  $\delta$ . Hence,  $\|\mathbf{x} - \tilde{\mathbf{x}}\|_2^2 \leq \delta$ . On the other hand, since  $\hat{\mathbf{x}} = \arg\min_{\mathbf{c} \in \mathcal{C}} \|\mathbf{y} - \sum_{i=1}^B \mathbf{D}_i \mathbf{c}_i\|_2^2$ , and  $\tilde{\mathbf{x}} \in \mathcal{C}$ ,  $\|\mathbf{y} - \sum_{i=1}^B \mathbf{D}_i \hat{\mathbf{x}}_i\|_2 \leq \|\mathbf{y} - \sum_{i=1}^B \mathbf{D}_i \tilde{\mathbf{x}}_i\|_2$ . But  $\mathbf{y} = \sum_{i=1}^B \mathbf{D}_i \mathbf{x}_i$ . Therefore,

$$\|\sum_{i=1}^{B} \mathbf{D}_{i}(\mathbf{x}_{i} - \hat{\mathbf{x}}_{i})\|_{2} \leq \|\sum_{i=1}^{B} \mathbf{D}_{i}(\mathbf{x}_{i} - \tilde{\mathbf{x}}_{i})\|_{2}.$$
 (13)

Note that, for a fixed  $c \in C$ ,

$$\|\sum_{i=1}^{B} \mathbf{D}_{i}(\mathbf{x}_{i} - \hat{\mathbf{x}}_{i})\|_{2}^{2} = \sum_{i=1}^{n} (\sum_{i=1}^{B} D_{ij}(x_{ij} - c_{ij}))^{2}$$
 (14)

Given a fixed x and c, for j = 1, ..., n, let

$$U_j = (\sum_{i=1}^{B} D_{ij}(x_{ij} - c_{ij}))^2.$$

 $U_1, \ldots, U_n$  are independent random variables and

$$E[U_j] = E\left[\sum_{i=1}^{B} \sum_{i'=1}^{B} D_{ij} D_{i'j} (x_{ij} - c_{ij}) (x_{i'j} - c_{i'j})\right]$$

$$= \sum_{i=1}^{B} \sum_{j=1}^{B} p^2 (x_{ij} - c_{ij}) (x_{i'j} - c_{i'j}) + \sum_{i=1}^{B} p (x_{ij} - c_{ij})^2$$

$$= p^{2} \left( \sum_{i=1}^{B} (x_{ij} - c_{ij})^{2} + (p - p^{2}) \sum_{i=1}^{B} (x_{ij} - c_{ij})^{2} \right).$$
 (15)

Given  $\epsilon_1 > 0$  and  $\epsilon_2 > 0$ ,  $\mathbf{x}_i \in \mathbb{R}^n$  and  $\mathbf{x} \in \mathbb{R}^{Bn}$ , define events  $\mathcal{E}_1$  and  $\mathcal{E}_2$  as

$$\mathcal{E}_{1} = \left\{ \frac{1}{n} \| \sum_{i=1}^{B} \mathbf{D}_{i}(\mathbf{x}_{i} - \tilde{\mathbf{x}}_{i}) \|_{2}^{2} \le \frac{p^{2}}{n} \| \sum_{i=1}^{B} (\mathbf{x}_{i} - \tilde{\mathbf{x}}_{i}) \|_{2}^{2} + \frac{p - p^{2}}{n} \| \mathbf{x} - \tilde{\mathbf{x}} \|_{2}^{2} + B\rho^{2} \epsilon_{1} \right\}$$
(16)

and

$$\mathcal{E}_{2} = \left\{ \frac{1}{n} \| \sum_{i=1}^{B} \mathbf{D}_{i}(\mathbf{x}_{i} - \mathbf{c}_{i}) \|_{2}^{2} \ge \frac{p^{2}}{n} \| \sum_{i=1}^{B} (\mathbf{x}_{i} - \mathbf{c}_{i}) \|_{2}^{2} + \frac{p - p^{2}}{n} \| \mathbf{x} - \mathbf{c} \|_{2}^{2} - B\rho^{2} \epsilon_{2} : \forall \mathbf{c} \in \mathcal{C} \right\},$$
(17)

respectively. Then, conditioned on  $\mathcal{E}_1 \cap \mathcal{E}_2$ , since  $\hat{\mathbf{x}} \in \mathcal{C}$  and  $\tilde{\mathbf{x}} \in \mathcal{C}$ , it follows from 13 that

$$\frac{p - p^2}{n} \|\mathbf{x} - \hat{\mathbf{x}}\|_2^2 \le \frac{p - p^2}{n} \|\mathbf{x} - \tilde{\mathbf{x}}\|_2^2 + \frac{p^2}{n} \|\sum_{i=1}^{B} (\mathbf{x}_i - \tilde{\mathbf{x}}_i)\|_2^2 + B\rho^2 \epsilon_1 + B\rho^2 \epsilon_2$$

$$\leq \frac{p + (B - 1)p^2}{n} \|\mathbf{x} - \tilde{\mathbf{x}}\|_2^2 + B\rho^2 \epsilon_1 + B\rho^2 \epsilon_2,\tag{18}$$

where the last line follows because  $\|\sum_{i=1}^{B} (\mathbf{x}_i - \tilde{\mathbf{x}}_i)\|_2^2 \leq B\|\mathbf{x} - \tilde{\mathbf{x}}\|_2^2$ . In the rest of the proof, we focus on bounding  $P(\mathcal{E}_1^c \cup \mathcal{E}_2^c)$ .

Note that since by assumption the  $\ell_{\infty}$ -norm of all signals in Q are upper-bounded by  $\rho/2$ ,  $U_i$ 's are also bounded as

$$U_{j} \leq \sum_{i=1}^{B} D_{ij}^{2} \cdot \sum_{i=1}^{B} (x_{ij} - c_{ij})^{2}$$

$$\leq \sum_{i=1}^{B} 1 \cdot \sum_{i=1}^{B} (\frac{\rho}{2} + \frac{\rho}{2})^{2} = B^{2} \rho^{2}.$$
(19)

Therefore, applying the Hoeffding's inequality,

$$P(\frac{1}{n}\sum_{j=1}^{n}U_{j} \ge \frac{1}{n}E[\sum_{j=1}^{n}U_{j}] + B\rho^{2}\epsilon_{1})$$

$$\le \exp(-\frac{2n^{2}B^{2}\rho^{4}\epsilon_{1}^{2}}{n(B^{2}\rho^{2})^{2}}) = \exp(-\frac{2n\epsilon_{1}^{2}}{B^{2}}).$$
(20)

Similarly,

$$P(\frac{1}{n}\sum_{i=j}^{n}U_{j} \leq \frac{1}{n}E[\sum_{j=1}^{n}U_{j}] - B\rho^{2}\epsilon_{2})$$

$$\leq \exp(-\frac{2n^{2}B^{2}\rho^{4}\epsilon_{2}^{2}}{n(B^{2}\rho^{2})^{2}}) = \exp(-\frac{2n\epsilon_{2}^{2}}{B^{2}}).$$
(21)

Therefore,

$$P(\mathcal{E}_1^c) \le \exp(-\frac{2n\epsilon_1^2}{B^2}) \tag{22}$$

and, by the union bound, since  $|\mathcal{C}| \leq 2^{Br}$ .

$$P(\mathcal{E}_2^c) \le 2^{Br} \exp(-\frac{2n\epsilon_2^2}{B^2}). \tag{23}$$

Again by the union bound,  $P(\mathcal{E}_1 \cap \mathcal{E}_2) \ge 1 - P(\mathcal{E}_1^c) - P(\mathcal{E}_2^c)$ . Given  $0 < \epsilon < \frac{16}{3}$ , the desired result follows by letting  $\epsilon_1 =$  $\epsilon_2 = \epsilon/2$ . Plug this into (7), and we have

Unlike in the proof of Theorem 1, 
$$\varphi(\mathbf{d}_1), \ldots, \varphi(\mathbf{d}_n)$$
 are no  $\frac{p-p^2}{n} \|\mathbf{x} - \hat{\mathbf{x}}\|_2^2 \le \frac{p+(B-1)p^2}{n} \|\mathbf{x} - \tilde{\mathbf{x}}\|_2^2 + B\rho^2 \epsilon_1 + B\rho^2 \epsilon_2$  longer independent. However, the expected values of  $\varphi(\mathbf{d}_j)$ 's are the same as those of  $U_j$ 's, because the dependencies are in-frame. Therefore,

Also, from 22 and 23, for  $\epsilon_1 = \epsilon_2 = B\epsilon/2$ ,

$$P(\mathcal{E}_1 \cap \mathcal{E}_2) \ge 1 - \exp(-\frac{2n\epsilon_1^2}{B^2}) - 2^{Br} \exp(-\frac{2n\epsilon_2^2}{B^2})$$
  
=  $1 - (2^{Br} + 1) \exp(-n\epsilon^2/2)$ .

Finally, to finish the proof, define

$$\delta' = \frac{\delta}{\rho^2 nB}.$$

Using this definition, minimizing the right hand side of (7) as a function of p, is equivalent to minimizing  $(1 + \frac{Bp}{1-p})\delta' +$  $\frac{B\epsilon}{(p-p^2)},$  which in turn is equivalent to minimizing

$$f(p) = \left(\frac{p}{1-p}\right)\delta' + \frac{\epsilon}{(p-p^2)}.$$

Note that  $f(0) = f(1) = \infty$ , which is consistent with our intuition that all-1 or an all-0 masks are not effective. Let  $p^*$ denote the value of  $p \in (0,1)$  that minimizes f(p), note that

$$f'(p) = \frac{1}{(1-p)^2} \delta' - \frac{1-2p}{(p-p^2)^2} \epsilon.$$
 (25)

Note that on one hand  $\lim_{p\to 0} f'(p) = -\infty$  and on the other hand  $f'(\frac{1}{2}) = 4\delta' > 0$ , which implies that  $p^*$  where  $f'(p^*) =$ 0 belongs to  $(0, \frac{1}{2})$ .

## B. Proof of Corollary 1

The proof follows similar to the proof of Theorem 1. The only difference is that, here,

$$E[U_j] = E\left[\sum_{i=1}^{B} \sum_{i'=1}^{B} D_{ij} D_{i'j} (x_{ij} - c_{ij}) (x_{i'j} - c_{i'j})\right]$$

$$= (2p - 1)^2 \left(\sum_{i=1}^{B} (x_{ij} - c_{ij}))^2 + 4(p - p^2) \sum_{i=1}^{B} (x_{ij} - c_{ij})^2.$$
(26)

## C. Proof of Theorem 2

Following the same steps as the initial steps of proof of

$$\sum_{j=1}^{n} \left(\sum_{i=1}^{B} D_{ij}(x_{ji} - \hat{x}_{ij})\right)^{2} \le \sum_{j=1}^{n} \left(\sum_{i=1}^{B} D_{ij}(x_{ij} - \tilde{x}_{ij})\right)^{2}$$

Define  $\mathbf{d}_j = [D_{1j}, \dots, D_{Bj}]$ . Note that  $\mathbf{d}_1, \dots, \mathbf{d}_n$  is a stationary first Markov process with state space  $S = \{0, 1\}^B$ such that

$$p(\mathbf{d}_i|\mathbf{d}_1,\ldots,\mathbf{d}_{i-1}) = p(\mathbf{d}_i|\mathbf{d}_{i-1}) = \prod_{j=1}^B p(d_{ij}|d_{(i-1)j}),$$

where  $p(d_{ij}|d_{(i-1)j})$  agrees with the transition probability of the Markov chain used for generating the masks. Given x and **c**, for j = 1, ..., n, let  $\varphi(\mathbf{d}_j) = (\sum_{i=1}^B D_{ij}(x_{ij} - c_{ij}))^2$ . Unlike in the proof of Theorem 1,  $\varphi(\mathbf{d}_1), \dots, \varphi(\mathbf{d}_n)$  are no are the same as those of  $U_i$ 's, because the dependencies are in-frame. Therefore,

$$E[\varphi(\mathbf{d}_j)] = p^2 (\sum_{i=1}^B (x_{ij} - c_{ij}))^2 + (p - p^2) \sum_{i=1}^B (x_{ij} - c_{ij})^2.$$

Similar to the proof of Theorem 1, define events  $\mathcal{E}_1$  and  $\mathcal{E}_2$ , as (16) and (17), respectively. To bound  $P((\mathcal{E}_1 \cap \mathcal{E}_2)^c)$ , we need to show the concentration of  $\sum_{j=1}^{n} \varphi(\mathbf{d}_{j})$  around its expected value. To achieve this goal, we use a result from [23], which is explained in Appendix A of the extended version of the paper [25]. To employ Theorem 5 in Appendix A, note that since the Markov chain is assumed to be stationary,  $\theta_1 = \theta_2 =$  $\dots = \theta_{n-1}$ . Therefore,

$$M_{n} = \max_{1 \leq i \leq n-1} (1 + \theta_{i} + \theta_{i}\theta_{i+1} + \dots + \theta_{i} \dots \theta_{n-1})$$

$$= 1 + \theta_{1} + \theta_{1}^{2} + \theta_{1}^{3} + \dots + \theta_{1}^{n-1}$$

$$= \frac{1 - \theta_{1}^{n}}{1 - \theta_{1}}.$$
(27)

To use theorem stated in Appendix A of [25], let c denote the Lipschitz coefficient of function  $\varphi: \mathcal{S} \to \mathbb{R}$ , defined earlier. Then, we have

$$P\left(\frac{1}{n}\sum_{j=1}^{n}\varphi(D_{j}) \geq \frac{1}{n}E\left[\varphi(D_{j})\right] + B\rho^{2}\epsilon_{1}\right)$$

$$\leq \exp\left(-\frac{n^{2}B^{2}\rho^{4}\epsilon_{1}^{2}}{2nc^{2}M_{n}^{2}}\right)$$

$$\leq \exp\left(-\frac{nB^{2}\rho^{4}\epsilon_{1}^{2}}{2c^{2}}(1-\theta_{1})^{2}\right), \tag{28}$$

and

$$P\left(\frac{1}{n}\sum_{j=1}^{n}\varphi(D_{j}) \leq \frac{1}{n}\operatorname{E}\left[\varphi(D_{j})\right] - B\rho^{2}\epsilon_{2}\right)$$

$$\leq \exp\left(-\frac{n^{2}B^{2}\rho^{4}\epsilon_{2}^{2}}{2nc^{2}M_{n}^{2}}\right)$$

$$\leq \exp\left(-\frac{nB^{2}\rho^{4}\epsilon_{2}^{2}}{2c^{2}}(1-\theta_{1})^{2}\right), \tag{29}$$

where in deriving both bounds we have used the fact that  $M_n = \frac{1-\theta_1^n}{1-\theta_1} \leq \frac{1}{1-\theta_1}$ . To bound the Lipschitz constant c, note that for and  $\mathbf{d}_j, \mathbf{d}_j' \in \{0,1\}^B$ , we have

$$\begin{aligned} |\varphi(\mathbf{d}_{j}) - \varphi(\mathbf{d}'_{j})| \\ &= |(\sum_{i=1}^{B} D_{ij}(x_{ij} - c_{ij}))^{2} - (\sum_{i=1}^{B} D'_{ij}(x_{ij} - c_{ij}))^{2}| \\ &= |\sum_{i=1}^{B} (D_{ij} + D'_{ij})(x_{ij} - c_{ij})| \cdot |\sum_{i=1}^{B} (D_{ij} - D'_{ij})(x_{ij} - c_{ij})| \\ &\leq 2B\rho^{2} d_{H}(\mathbf{d}_{j}, \mathbf{d}'_{j}), \end{aligned}$$
(30)

where (a) follows because for all  $\mathbf{x} \in \mathcal{Q}$ ,  $\|\mathbf{x}\|_{\infty} \leq \frac{\rho}{2}$ . This implies that  $c \geq 2B\rho^2$ . Finally, setting  $\epsilon_1 = \epsilon_2 = \epsilon/2$ , and noting that  $|\mathcal{C}| \leq 2^{Br}$  yields the desired result.

# D. Proof of Theorem 3

Again we follow the same steps as the initial steps of proof of Theorem 1 to derive  $\sum_{j=1}^n (\sum_{i=1}^B D_{ij}(x_{ji} - \hat{x}_{ij}))^2 \le \sum_{j=1}^n (\sum_{i=1}^B D_{ij}(x_{ij} - \tilde{x}_{ij}))^2$ . As in the proof of Theorem 2, define  $\mathbf{d}_j = [D_{1j}, \ldots, D_{Bj}]$ . Unlike the proof of Theorem 2, here  $\mathbf{d}_1, \ldots, \mathbf{d}_n$  are independent and identically distributed. Again similar to the proof of Theorem 1, given  $\mathbf{x}$  and  $\mathbf{c}$ , for  $j=1,\ldots,n$ , define

$$U_j(\mathbf{x}, \mathbf{c}) = (\sum_{i=1}^B D_{ij}(x_{ij} - c_{ij}))^2.$$

Note that  $U_1(\mathbf{x}, \mathbf{c}), \dots, U_n(\mathbf{x}, \mathbf{c})$  are independent random variables. Moreover, they are positive and bounded with the same upper bound as the one derived in (19). Therefore, we can still apply the Hoeffding's inequality and derive (20) and (21). The key difference now is that computing  $\mathrm{E}[U_j(\mathbf{x}, \mathbf{c})]$  is more complex as the entries of  $\mathbf{d}_j$  are not independent.

To compute  $E[U_j(\mathbf{x}, \mathbf{c})]$ , define  $\mu_{ij} = x_{ij} - c_{ij}$ . Also, note that as before,  $E[D_{ij}^2] = E[D_{ij}] = p$ . Moreover,

$$E[U_j(\mathbf{x}, \mathbf{c})] = E[(\sum_{i=1}^B D_{ij}(x_{ij} - c_{ij}))^2]$$

$$= \sum_{i_1=1}^B \sum_{i_2=1}^B E[D_{i_1j}D_{i_2j}]\mu_{i_1j}\mu_{i_2j}.$$
(31)

Without loss of generality, assume that  $i_1 < i_2$ . Then,  $\mathrm{E}[D_{i_1j}D_{i_2j}] = \mathrm{P}(D_{i_1j} = D_{i_2j} = 1) = \mathrm{P}(D_{i_1j} = 1)$   $\mathrm{P}(D_{i_2j} = 1|D_{i_1j} = 1)$ . To compute  $\mathrm{P}(D_{i_2j} = 1|D_{i_1j} = 1)$ , we need to compute  $(i_2-i_1)$ -th order transition probability of the Markov chain. The transition kernel of the Markov chain can be written as

$$P = \begin{bmatrix} 1 - q_0 & q_0 \\ q_1 & 1 - q_1 \end{bmatrix}.$$

Let  $Q=egin{bmatrix} 1 & -q_0 \\ 1 & q_1 \end{bmatrix}$ , and let  $\alpha=1-q_0-q_1.$  Then,

$$\Pi = Q \begin{bmatrix} 1 & 0 \\ 0 & \alpha \end{bmatrix} Q^{-1} \tag{32}$$

Using this representation, the *k*-th order transition probability of this Markov chain can be written as

$$\Pi^{k} = \frac{1}{q_0 + q_1} \begin{bmatrix} q_1 & q_0 \\ q_1 & q_0 \end{bmatrix} + \frac{\alpha^{k}}{q_0 + q_1} \begin{bmatrix} q_0 & -q_0 \\ -q_1 & q_1 \end{bmatrix}.$$
(33)

Therefore, for  $k = 1, \ldots, n - i$ 

$$P(D_{(i+k)j} = 1 | D_{ij} = 1) = \frac{q_0 + \alpha^k q_1}{q_0 + q_1} = p + (1-p)\alpha^k.$$

Thus.

$$E[U_{j}(\mathbf{x}, \mathbf{c})] = \sum_{i_{1}}^{B} \sum_{i_{2}}^{B} E[D_{i_{1}j}D_{i_{2}j}]\mu_{i_{1}j}\mu_{i_{2}j}$$

$$= \sum_{i_{1}}^{B} \sum_{i_{2}}^{B} p(p + (1 - p)\alpha^{|i_{1} - i_{2}|})\mu_{i_{1}j}\mu_{i_{2}j}$$

$$= p^{2}(\sum_{i}^{B} \mu_{ij})^{B} + p(1 - p)\sum_{i_{1}}^{B} \sum_{i_{2}}^{B} \alpha^{|i_{1} - i_{2}|}\mu_{i_{1}j}\mu_{i_{2}j}$$

$$= p^{2}(\sum_{i}^{B} \mu_{ij})^{B} + p(1 - p)\mu_{j}^{T}\Lambda\mu_{j}, \tag{34}$$

where  $\mu_j = [\mu_{1j}, \dots, \mu_{Bj}]^T$  and  $\Lambda$  is defined in (12). Therefore,  $E[U_j(\mathbf{x}, \mathbf{c})]$  can be upper- and lower-bounded as

$$E[U_j(\mathbf{x}, \mathbf{c})] \le p^2 (\sum_{i=1}^B \mu_{ij})^2 + p(1-p)\lambda_{\max}(\Lambda) \|\boldsymbol{\mu}_j\|_2^2,$$
 (35)

and

$$E[U_j(\mathbf{x}, \mathbf{c})] \ge p^2 (\sum_{i=1}^B \mu_{ij})^2 + p(1-p)\lambda_{\min}(\Lambda) \|\boldsymbol{\mu}_j\|_2^2.$$
 (36)

Define.

$$\mathcal{E}_1 = \{ \sum_{j=1}^n U_j(\mathbf{x}, \mathbf{c}) \ge \sum_{j=1}^n \mathrm{E}[U_j(\mathbf{x}, \mathbf{c})] - B\rho^2 \epsilon_1, \ \forall \mathbf{c} \in \mathcal{C} \},$$

and

$$\mathcal{E}_2 = \{ \sum_{j=1}^n U_j(\mathbf{x}, \tilde{\mathbf{x}}) \le \sum_{j=1}^n \mathrm{E}[U_j(\mathbf{x}, \tilde{\mathbf{x}})] + B\rho^2 \epsilon_2, \},$$

respectively. As explained earlier, we the bounds in (20) and (21) still hold here too. Therefore, the lower bound on  $\mathcal{E}_1 \cap \mathcal{E}_2$  is the same as before. But conditioned on  $\mathcal{E}_1 \cap \mathcal{E}_2$ , employing the bounds in (35) and (36), it follows that

$$\begin{split} & \frac{p(1-p)\lambda_{\min}(\Lambda)}{n} \|\mathbf{x} - \hat{\mathbf{x}}\|_{2}^{2} \\ & \leq \frac{p(1-p)\lambda_{\max}(\Lambda)}{n} \|\mathbf{x} - \tilde{\mathbf{x}}\|_{2}^{2} + \frac{p^{2}}{n} \|\sum_{i=1}^{B} (\mathbf{x}_{i} - \tilde{\mathbf{x}}_{i})\|_{2}^{2} \\ & + B\rho^{2}\epsilon_{1} + B\rho^{2}\epsilon_{2} \\ & \leq \frac{p(1-p)\lambda_{\max}(\Lambda) + p^{2}B}{n}\delta + B\rho^{2}\epsilon, \end{split}$$

where the last line follows by setting  $\epsilon_1 = \epsilon_2 = \frac{\epsilon}{2}$ .

## E. Proof of Corollary 2

According to the Gershgorin circle theorem [24], since all the diagonal entries of  $\Lambda$  are equal to one, every eigenvalue of  $\Lambda$  lies within at least one of the Gershgorin discs. These discs are all centered at one and have radii equal to

$$r_i = \sum_{j \neq i} \Lambda_{ij},$$

for  $i = 1, \dots, B$ . Therefore,

$$1 - \max_{i} r_i \le \lambda_{\min}(\Lambda) \le \lambda_{\max}(\Lambda) \le 1 + \max r_i.$$

But

$$\max r_i \le 2(\alpha + \alpha^2 + \ldots) = \frac{2\alpha}{1 - \alpha}.$$

Therefore,

$$\frac{1-3\alpha}{1-\alpha} \le \lambda_{\min}(\Lambda) \le \lambda_{\max}(\Lambda) \le \frac{1+\alpha}{1-\alpha}.$$

Inserting these bounds in the result of Theorem 3 yields the desired result.

## VI. CONCLUSION

In this paper, we have theoretically studied the performance of SCI systems under different types of binary masks. Prior art had characterized the theoretical performance of SCI systems under i.i.d. Gaussian masks. However, in practice the masks are rarely i.i.d. Gaussian. In many applications, the masks are binary-valued. Moreover, there have been results in the literature on optimizing binary masks such that the performance of SCI system is optimized. In this paper, we have characterized the performance of SCI systems under three different models for binary masks. Our results theoretically confirm the observations in the literature that for i.i.d. binary masks to optimize the performance the probability of 1s should be smaller than 0.5.

#### ACKNOWLEDGMENTS

This research was supported by the U.S. National Science Foundation grant CCF-2237538.

#### REFERENCES

- Z. Liu, H. Wang, and Q. Li. Tongue tumor detection in medical hyperspectral images. Sensors, 12(1):162–174, 2011.
- [2] Guolan Lu and Baowei Fei. Medical hyperspectral imaging: a review. J. of Bio. Opt., 19(1):010901, 2014.
- [3] E. K. Hege, D. O'Connell, W. Johnson, S. Basty, and E. L. Dereniak. Hyperspectral imaging for astronomy and space surveillance. In *Ima. Spec. IX*, volume 5159, pages 380–391. SPIE, 2004.
- [4] Tobias H Kurz, Simon J Buckley, and John A Howell. Close-range hyperspectral imaging for geological field studies: workflow and methods. Int. J. of Remote Sensing, 34(5):1798–1822, 2013.
- [5] S. Peyghambari and Y. Zhang. Hyperspectral remote sensing in lithological mapping, mineral exploration, and environmental geology: an updated review. *J. of App. Rem. Sen.*, 15(3):031501, 2021.
- [6] M. E. Gehm, R John, D. J Brady, R. M Willett, and T. J. Schulz. Single-shot compressive spectral imaging with a dual-disperser architecture. Opt. Exp., 15(21):14013–14027, 2007.
- [7] X. Yuan, D. J. Brady, and A. K. Katsaggelos. Snapshot compressive imaging: Theory, algorithms, and applications. *IEEE Sig. Proc. Mag.*, 38(2):65–88, 2021.
- [8] W. Saideni, D. Helbert, F. Courrèges, and J. P. Cances. An Overview on Deep Learning Techniques for Video Compressive Sensing. *App. Sci.*, 12(5), Mar. 2022.
- [9] M. Qiao, Z. Meng, J. Ma, and X. Yuan. Deep learning for video compressive sensing. APL Photonics, 5(3):030801, 2020.
- [10] Z. Meng, S. Jalali, and X. Yuan. Gap-net for snapshot compressive imaging. arXiv preprint arXiv:2012.08364, 2020.
- [11] X. Yuan, Y. Liu, J. Suo, F. Durand, and Q. Dai. Plug-and-play algorithms for video snapshot compressive imaging. *IEEE Trans. on Pat. Ana. and Mach. Int.*, 44(10):7093–7111, 2022.
- [12] L. Wang, M. Cao, Y. Zhong, and X. Yuan. Spatial-temporal transformer for video snapshot compressive imaging, 2022.
- [13] Shirin Jalali and Xin Yuan. Snapshot compressed sensing: Performance bounds and algorithms. *IEEE Trans. Inform. Theory*, 65(12):8005–8024, 2019.

- [14] P. Llull, X. Liao, X. Yuan, J. Yang, D. Kittle, L. Carin, G. Sapiro, and D. J. Brady. Coded aperture compressive temporal imaging. *Opt. Exp.*, 21(9):10526–10545, 2013.
- [15] S. Jalali and A. Maleki. From compression to compressed sensing. Appl. Comp. Harmonic Anal. (ACHA), 40(2):352–385, 2016.
- [16] M. Iliadis, L. Spinoulas, and A. K. Katsaggelos. Deepbinarymask: Learning a binary mask for video compressive sensing. *Dig. Sig. Proc.*, 96:102591, 2020.
- [17] X. Zhang, Y. Zhang, R. Xiong, Q. Sun, and J. Zhang. Herosnet: Hyperspectral explicable reconstruction and optimal sampling deep network for snapshot compressive imaging. In *Proc. of the IEEE/CVF Conf. on Comp. Vis. and Pat. Rec. (CVPR)*, pages 17532–17541, June 2022.
- [18] R. Koller, L. Schmid, N. Matsuda, T. Niederberger, L. Spinoulas, O. Cossairt, G. Schuster, and A. K. Katsaggelos. High spatio-temporal resolution video with compressed sensing. *Opt. Exp.*, 23(12):15992– 16007, 2015.
- [19] Z. Zhang, C. Deng, Y. Liu, X. Yuan, J. Suo, and Q. Dai. Ten-mega-pixel snapshot compressive imaging with a hybrid coded aperture. *Pho. Res.*, 9(11):2277, Oct. 2021.
- [20] Y. Li, M. Qi, R. Gulve, M. Wei, R. Genov, K. N. Kutulakos, and W. Heidrich. End-to-end video compressive sensing using andersonaccelerated unrolled networks. In 2020 IEEE International Conference on Computational Photography (ICCP), pages 1–12, 2020.
- [21] A. Wagadarikar, N. Pitsianis, X. Sun, and D. Brady. Video rate spectral imaging using a coded aperture snapshot spectral imager. *Opt. Express*, 17(8):6368–6388, Apr. 2009.
- [22] F. E. Rezagah, S. Jalali, E. Erkip, and H. V. Poor. Compression-based compressed sensing. *IEEE Trans. Inform. Theory*, 63(10):6735–6752, Oct. 2017
- [23] L. A. Kontorovich and K. Ramanan. Concentration inequalities for dependent random variables via the Martingale method. *Ann. of Prob.*, 36(6):2126–2158, 2008.
- [24] S. A. Gershgorin. Uber die abgrenzung der eigenwerte einer matrix. Bull. Acad. Sci. l'URSS. Classe des Sci. Math., (6):749–754, 1931.
- [25] M. Zhao and S. Jalali. Theoretical analysis of binary masks in snapshot compressive imaging systems. arXiv preprint arXiv:2307.07796, 2023.